Vision Research, Vol. 18, pp. 959–969

0042-6989/78/0801-0959$02.00/0

SPACE DOMAIN PROPERTIES OF A SPATIAL FREQUENCY CHANNEL IN HUMAN VISION

GORDON E. LEGGE[1]

The Physiological Laboratory, University of Cambridge, Cambridge CB2 3EG, England

(*Received* 22 *February* 1977; *in revised form* 6 *October* 1977)

Abstract—Many properties of contrast detection in human vision may be described with reference to a set of tuned spatial frequency channels. The spatial sensitivity of the channel with optimal sensitivity at 3.0 c/deg was studied by measuring threshold as a function of the width of truncated 3.0 c/deg sine-wave gratings that ranged from 2.3′ to 4.6°. Three strategies were used to isolate the threshold response of the channel: (1) The channel at 3.0 c/deg was chosen because of its position at the peak of the contrast sensitivity function. (2) A discrimination paradigm was used in which test stimuli were superimposed on a low contrast grating which was shown to selectively facilitate their detection. (3) The detecting channel was more sensitive to the sine-wave configuration of the test stimuli than to more conventional spatial summation stimuli, such as rectangular bars. Results of the main experiment showed that threshold contrasts for the truncated sine-wave stimuli declined in two stages. From 2.3′ to 40′, the threshold decline was steep, with a plateau at 10′. From 40′ to 4.6°, threshold declined as a power function of stimulus width with an exponent of −0.35. The data of the main experiment were used to derive the spatial receptive field sensitivity for the channel at 3.0 c/deg. The data were accounted for by spatial summation within a receptive field, and probability summation in space across receptive fields.

Key Words—spatial frequency; sine-wave gratings; contrast sensitivity function; spatial summation; probability summation.

INTRODUCTION

Contrast sensitivity in human vision may be represented by the contrast sensitivity function—the relation between threshold contrast for sine-wave grating targets and their spatial frequencies (Schade, 1956). If linearity is assumed, this function can be used to predict visual thresholds for arbitrary patterns. Although the assumption of linearity is inappropriate for suprathreshold contrast (Legge, 1976a), small signal linearity holds for the detection of periodic patterns (Campbell and Robson, 1968) and large classes of aperiodic patterns (Campbell, Carpenter and Levinson, 1969; Hines, 1976).

Campbell and Robson (1968) proposed that the contrast sensitivity function is an envelope for a set of constituent, independent spatial frequency sensitivity functions. Each of these, ascribed to a spatial frequency channel, has narrower spatial frequency sensitivity than the visual system as a whole, and optimal sensitivity reflected by its position on the contrast sensitivity function.

Models of contrast detection using only the contrast sensitivity function have been termed "single channel" models, and those assuming the existence of a set of spatial frequency channels have been termed "multiple channels" models (Graham and Nachmias, 1971). Although the former are adequate for many purposes, experiments showing spatial frequency selective effects demonstrate a need for the additional assumptions of the latter. These experiments include evidence for critical band masking in vision (Stromeyer and Julesz, 1972), the independent detection of first and third harmonics (Graham and Nachmias, 1971), and spatial frequency adaptation (Pantle and Sekuler, 1968; Blakemore and Campbell, 1969). Spatial frequency adaptation is the increase in contrast threshold for the detection of a sine-wave grating following prolonged exposure to a similar sine-wave grating of high contrast. Blakemore and Campbell (1969) observed that, for adaptation to gratings of 3.0 c/deg and above, threshold elevation peaked at the adapting frequency, and was confined to a limited band of spatial frequencies surrounding it. The spatial frequency tuning curve represents the effects of adaptation at one frequency on channels at several test frequencies, but it may be used to derive the spatial frequency sensitivity of the channel at the adapting frequency (Stromeyer and Klein, 1974). Accordingly, spatial frequency adaptation has been used as a technique for the isolation and examination of the frequency response of individual spatial frequency channels.

Under the assumption of small signal linearity, Fourier transformation of the contrast sensitivity function yields its space domain equivalent—the line-spread function of the visual system. (In view of inhomogeneities in contrast sensitivity across the visual field, the line-spread function so derived will depend upon the location, size and orientation of the grating patch by which the contrast sensitivity function was measured. To the extent that contrast sensitivity may be approximated as uniform across the patch, the Fourier transform may be used quantitatively to derive the line-spread function from the contrast sensitivity function. If inhomogeneities are taken into

[1] Send reprint requests to the author at the Department of Psychology, University of Minnesota, 75 East River Road, Minneapolis, Minnesota 55455, U.S.A.

account, corrections to the line-spread function so computed will be necessary.) Direct, space domain measurements of the line-spread function of the visual optics have been made using double passage ophthalmoscopic techniques (Westheimer and Campbell, 1962; Krauskopf, 1962; Campbell and Gubisch, 1966). The line-spread function of the entire visual system depends upon both the quality of the visual optics and the properties of the subsequent neural processing (Campbell and Green, 1965).

Under the assumptions of a multiple channels model, Fourier transformation of the spatial frequency tuning curves of the set of independent channels yields a set of line-spread functions. These are weighting functions which represent the space domain sensitivity of the spatial frequency channels. In this paper, these functions will be called "receptive fields", after possible underlying neural mechanisms. (Although this term is used in electrophysiology to refer to spatial response properties of single cells, characteristics of receptive fields measured psychophysically are undoubtedly due to populations of cells, perhaps in a number of visual centers.) An alternative formulation of the multiple channels model can be made in terms of a set of receptive fields (Thomas, 1970; Macleod and Rosenfeld, 1974; Legge, 1976a). In the space domain, the term "channel" will be used to refer collectively to all receptive fields with the same weighting function. It is assumed that the receptive fields vary in spatial structure (corresponding to their different frequency selectivity), in position in visual coordinates (providing a means for phase encoding), and in orientation sensitivity. In a linear formulation, it is assumed that the response of an individual unit is proportional to the convolution of its receptive field and the stimulus luminance distribution.

Just as measurements in the frequency domain may depend on the response of many spatial frequency channels, e.g. the contrast sensitivity function, measurements in the space domain may depend on the response of many receptive fields. It is important to find strategies for isolating the response of particular receptive field types in order to study their spatial properties.

Several authors have obtained space domain sensitivity weighting functions without attempting to isolate component responses. Graham, Brown and Mote (1939) and Matin (1975) have attempted to account for areal summation data in the detection of spots with the use of spatial weighting functions. Blackwell and his colleagues (Kincaid, Blackwell and Kristofferson, 1960; Blackwell, 1963) have studied contrast threshold as a function of the diameter of test spots. The derivative of the resulting areal summation function is a sensitivity profile which they have termed an "element contribution function". Westheimer (1965, 1967) measured increment thresholds for small, flashing test spots at the center of circular backgrounds of varying diameter, at scotopic and photopic levels, respectively. From these measurements, he obtained sensitivity profiles relating increment threshold to background diameter. Thomas (1968) derived sensitivity profiles from measurements of the perceived brightness of a 3′ test line as a function of the position of low contrast, but suprathreshold, inducing lines. Westheimer and Wiley (1970), working at scotopic levels, obtained an analogous sensitivity profile by measuring increment threshold for a 0.1° diameter test spot as a function of the position of one or more suprathreshold inducing spots. Fiorentini (1971) and Hines (1976) have derived sensitivity profiles from measurements of the threshold contrast for narrow test lines as a function of their separation from subthreshold inducing lines.

All of these studies treat the visual system as a single channel, and the resulting sensitivity profiles are therefore characteristic of the visual system as a whole. The relative contributions of receptive fields of different shape cannot be specified.

Bagrash (1973) has attempted to isolate the spatial response of individual receptive fields. Following adaptation to luminous spots of one diameter, subjects appeared to show a decreased sensitivity in the areal summation function for test spots of similar size. Kulikowski and King-Smith (1973) have studied the effects of a variety of subthreshold patterns on the detectability of lines, edges and gratings. They have associated separate channels with the detection of each test configuration. By measuring threshold reduction for the test stimuli as a function of the spatial configuration of subthreshold patterns, they have inferred spatial sensitivities for these channels.

In the context of the multiple channels model, the purposes of the present research were to isolate a single channel and to examine its space domain properties. These properties include the shape of the channel's receptive fields, and the means by which the responses of these receptive fields are combined in the detection of stimulus patterns.

Three strategies were used to render the channel in question differentially sensitive so that its response characteristics would be reflected in contrast threshold measurements. These strategies, to be discussed later, were: (1) picking the channel at the peak of the contrast sensitivity function; (2) use of a discrimination paradigm; (3) matching the waveforms of the test stimuli to the anticipated shape of the channel's receptive fields.

Using these three strategies to isolate channel response, contrast threshold as a function of width was measured for truncated sine-wave grating test targets. The luminance profiles of several are shown by the solid lines in Fig. 1. From these measurements, a receptive field profile was derived.

METHOD

Apparatus

Vertical sine-wave gratings were generated on a Tektronix 502 oscilloscope with a P2 bluish-green phosphor by *z*-axis modulation (Schade, 1956; Campbell and Green, 1965). The mean luminance of the circular display was kept constant at 4.6 cd/m^2.

Two sinusoidal voltages could be applied simultaneously to the oscilloscope. Each was produced by an Intercil 5038 function generator. The frequency, amplitude and timing of the signals were controlled by a PDP-4 computer through 8-bit Precision Monolithics DAC-08 D/A converters. Patterns consisting of the superposition of two sine-wave modulations, each with adjustable spatial frequency, contrast, phase, spatial position and width on the screen, could be generated at a frame rate of 1 msec. The function generators could be bypassed in order to apply

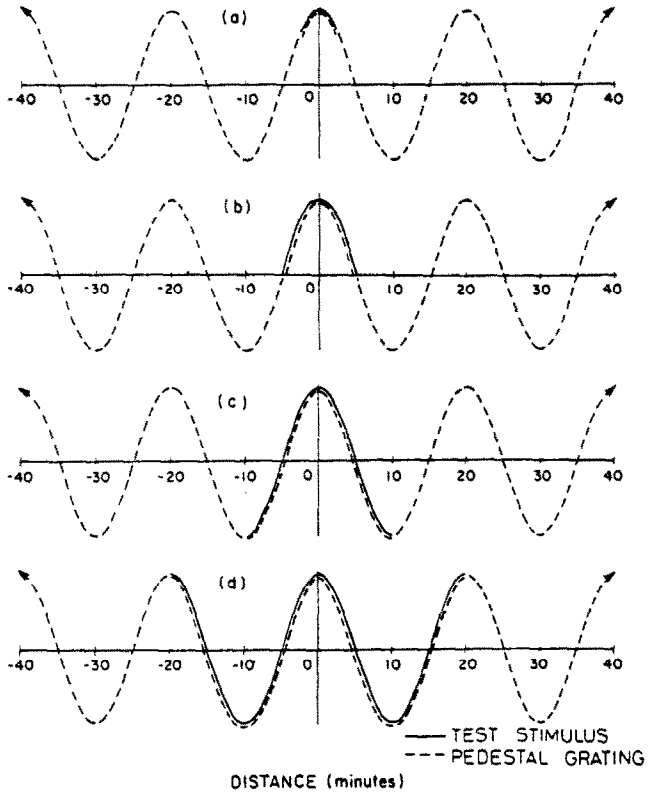

Fig. 1. Luminance profiles for 4 sets of stimuli are shown. The abscissa lies at the mean luminance level. Dashed curves represent the 3.0 c/deg full-field pedestal gratings. Solid curves represent the truncated sine-wave test stimuli of widths: (a) 5′ = 0.25 cycles; (b) 10′ = 0.5 cycles; (c) 20′ = 1.0 cycle; (d) 40′ = 2.0 cycles.

d.c. pulses to the oscilloscope to produce vertical bar stimuli. a.c. coupling in the z-axis circuit meant that only bars of a limited width could be produced without noticeable distortion. Timing was accurately controlled by a 1 kHz crystal clock in the computer. The contrast of the patterns could also be controlled by a hand-held potentiometer. The computer sequenced stimulus presentations and collected data.

The contrast of all patterns is defined as the ratio of peak luminance to the mean luminance of 4.6 cd/m^2. All signals had contrasts well below 0.3, the level at which sine-wave gratings exhibited nonlinear distortion.

The display was 5° in diameter from a viewing distance of 114 cm, and had a dark surround. The function relating contrast to z-axis voltage and frequency was measured with a scanning slit and photometer.

Subjects viewed the display monocularly through a 3 mm artificial pupil, with their heads supported by a chin rest. They were instructed to fixate a small, black spot at the center of the screen during the 250 msec signal exposures. Under these conditions, the median distance of involuntary eye movements is less than 1′ (Riggs, Armington and Ratliff, 1954).

Experimental procedure

Each experimental session began with 5–10 min light adaptation to the uniform display. Blocks of 55 trials in a temporal two-alternative forced-choice staircase procedure (Wetherill and Levitt, 1964) were used to obtain estimates of the 71% correct signal contrasts. For details, see Legge (1978). The threshold measure was the geometric mean of these estimates. The error bars in Figs 3 and 4 correspond to ±1 standard error of the mean. The geometric mean was used because standard errors appeared roughly constant in logarithmic units. There were small differences in overall sensitivity between subjects, and slight, irregular scale changes in sensitivity from day to day for individual subjects. Accordingly, prior to averaging, threshold estimates were normalized by the geometric mean of all threshold estimates obtained during the session. After averaging, the result was rescaled by the grand mean.

Subjects

There were three female subjects of college age. AA and JK are emmetropic. WWL has been optically corrected.

RESULTS AND DISCUSSION

Isolating the response of a spatial frequency channel

Three strategies were used to isolate a spatial frequency channel so that its space domain properties could be examined.

(1) *Channel at the peak of the contrast sensitivity function.* Typical measurements of the contrast sensitivity function at moderate photopic luminances exhibit a bandpass characteristic with optimal sensitivity (lowest threshold) near 2.0–5.0 c/deg. If the peak of the contrast sensitivity function is assumed to be due to spatial frequency channels of the greatest sensitivity, it will be easiest to isolate the spatial response of these channels because they are already optimally sensitive.

Figure 2 shows contrast sensitivity functions for the three subjects. The functions labelled "many-cycle" resulted from the detection of test gratings subtending 4.6° and the one labelled "one-cycle" resulted from single cycles of the specified spatial frequency. Data of subject WWL have been shifted upward by 0.3 log units (a factor of 2) and data of JK downward by 0.1 log units (a factor of 1.26).

Data points for the many-cycle functions are single threshold estimates obtained from a block of 55 trials with the forced choice procedure in one session. For the one-cycle function, each data point is the mean of two such estimates. The smooth curves are the best fitting cubic polynomials (least-squares criterion) through the sets of data.

For all curves, lowest thresholds were achieved at or near 3.0 c/deg. This is true for both the broad "many-cycle" targets and the narrow "one-cycle" targets. It was therefore assumed that, for the stimulus conditions of these experiments, spatial frequency channels at 3.0 c/deg were optimally sensitive. Accordingly, truncated sine-wave gratings of 3.0 c/deg were chosen as the stimulus set for the main experiment.

Notice that the low frequency attenuation in sensitivity is present for the one-cycle function, although it is somewhat shallower than for the others. Hoekstra, van der Goot, van den Brink and Bilsen (1974), and Savoy and McCann (1975) have reported results supporting the suggestion that the low frequency attenuation is an artifact of a decreased number of cycles in low spatial frequency test stimuli. However, Estevez and Cavonius (1976) have shown that equal-cycle contrast sensitivity functions all have approximately the same shape. Low frequency attenuation has been reported for one-cycle targets in sine phase (Campbell, Carpenter and Levinson, 1969) and for half-cycle targets in cosine phase (Hines, 1976). As will be reported below, increasing the number of cycles of a sine-wave target does systematically lower threshold, and accounts for the relatively greater low frequency attenuation of the many-cycle targets in Fig. 2.

(2) *Use of a discrimination paradigm.* In a discrimination paradigm, an observer must discriminate between stimuli of intensities I and $I + \Delta I$. The increment signal ΔI is varied to determine threshold, while the base, or "pedestal", intensity I is kept constant. In two-alternative forced choice, for instance, the pedestal is presented in both exposure intervals, but the signal is presented in only one. Absolute detection occurs when the pedestal intensity is 0. Often, there is a range of low pedestal intensities for which the incremental threshold is lower than the absolute threshold—that is, discrimination is better than absolute detection. This is true for the discrimination of luminance increments (Nachmias and Kocher, 1970; Cohn, Thibos and Kleinstein, 1974), and for grating contrast discrimination (Nachmias and Sansbury, 1974).

Data illustrating the pedestal effect are shown in Fig. 3(a). Means for 3 threshold estimates for the detection of a 3.0 c/deg signal grating are plotted as a function of the contrast of an identical pedestal grating. For the range of pedestal contrasts shown, the signal thresholds decrease systematically with increasing pedestal contrast. (For larger pedestal contrasts, the relation is reversed, and signal thresholds increase with increasing pedestal contrasts. This effect is often termed "masking".)

The pedestal effect is frequency selective. In Fig. 3(b), thresholds for 3.0 c/deg grating signals are plotted as a function of the frequency of constant contrast pedestal gratings. (The signal and pedestal were always in cosine phase at the fixation point.) The lowering of signal threshold is produced by pedestals differing in frequency by no more than 0.5 octaves from the signal frequency.

Legge (1976b) has used a discrimination paradigm to demonstrate that a 3.0 c/deg sine-wave grating pedestal will also facilitate the detection of 2.3' (fine line) and 20' (one-cycle) truncated sine-wave grating targets, and that the effect is greatest for a 3.0 c/deg pedestal, even for the fine line. These findings indicate that the mechanisms detecting the truncated sine-wave targets are tuned to 3.0 c/deg.

The frequency selectivity of the pedestal effect makes

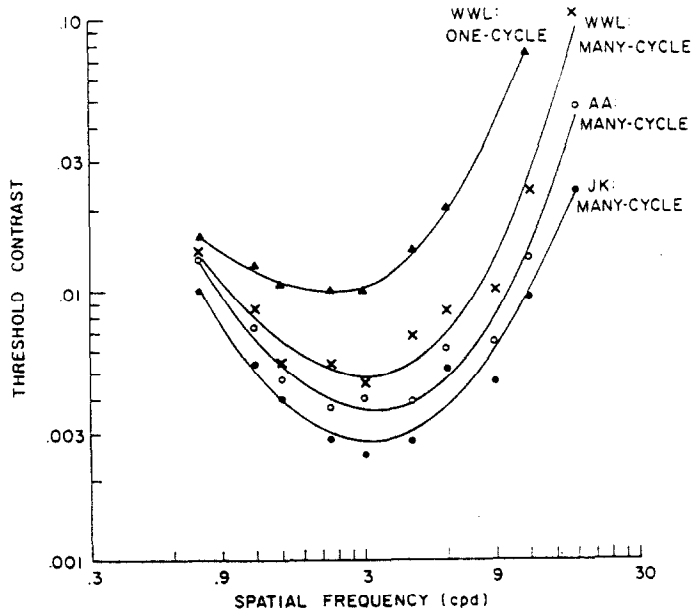

Fig. 2. Contrast threshold functions. Contrast threshold was measured as a function of spatial frequency for sine-wave gratings. Many-cycle targets subtended 4.6°. Each data point was based on a block of 55 forced-choice trials. One-cycle targets contained a single cycle (cosine phase) at the indicated spatial frequency. Data points are the means of threshold estimates obtained from two blocks of 55 forced choice trials. The smooth curves are best fitting cubic polynomial functions (least-squares criterion). Data are shown for three subjects: (●) JK displaced downward by 0.1 log units; (○) AA; (×, ▲) WWL, displaced upward by 0.3 log units.

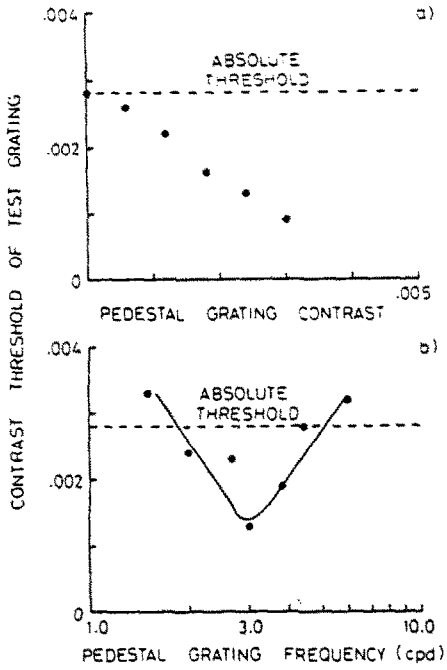

Fig. 3. The pedestal effect. Threshold contrasts for a 3.0 c/deg test grating, presented in one exposure of a forced-choice trial, was measured as a function of (a) the contrast, and (b) the spatial frequency, of a "pedestal" grating, presented in both exposures. In (a), the frequency of the pedestal was 3.0 c/deg, and in (b) its contrast was 0.0024. Data points are means of 3 threshold estimates, each from a block of forced-choice trials. Horizontal dashed lines represent threshold contrast in the absence of the pedestal grating. A smooth curve has been drawn through the data points in (b). Test gratings and pedestal gratings were always in cosine phase with the fixation point.

the discrimination paradigm useful in isolating the response of the 3.0 c/deg channel. The data of Fig. 3, and the evidence cited from Legge (1976b), indicate that a 3.0 c/deg grating pedestal differentially sensitizes the 3.0 c/deg channel so that the truncated sine-wave grating test stimuli are detected by it. Hence, a discrimination paradigm was used in the main experiment. A 3.0 c/deg pedestal grating at the subject's threshold contrast was presented in both intervals of the forced-choice trial, but the test stimulus was presented in only one. The subject's task was to discriminate test-plus-pedestal from pedestal alone.

(3) *Configuration of the test stimulus.* A variety of receptive field functions are consistent with a given spatial frequency tuning curve. If more than one of the detector types exists in the visual system (e.g. asymmetrical edge detectors and symmetrical center-surround "bar" detectors) the configuration of the stimulus will determine which is optimally stimulated. A stimulus, optimally matched in shape to the receptive field, will preferentially stimulate it. In view of the ubiquitous center-surround organization revealed by electrophysiological studies of vertebrate vision, test stimuli which may be roughly matched in form have been chosen—namely, segments of sine-wave gratings. In cosine phase with the center of an optimal center-surround receptive field, the positive half-cycle will stimulate the excitatory center while the negative half-cycle will be aligned with the inhibitory flanks. (Edge sensitive mechanisms are also known to exist in vertebrate vision. If they had been the objects of investigation, segments of sine-wave gratings in sine phase would have been appropriate.) It was assumed that the sine-wave test stimuli would be better matched to the form of the target receptive fields than more conventional configurations, such as circular spots or bars. To check this, threshold contrasts for rectangular, light bars were measured as a function of bar width, and compared with corresponding thresholds for the grating stimuli.

In Fig. 4, threshold contrasts for rectangular bars (triangles) and truncated sine-waves (filled circles and crosses) are plotted as a function of their width. The latter will be discussed below. The former represent geometric means of 4 threshold estimates, 2 each from subjects AA and JK. Each estimate was obtained from a block of 55 forced-choice trials.

Thresholds for the rectangle and sine-wave grating stimuli are very similar for widths up to 12', whereupon the rectangle curve flattens out. Beyond 12', the sine-wave curve continues to drop, rapidly falling below the rectangle curve. Similar results for rectangles have been presented by Shapley (1974), Hines (1976) and Kulikowski and King-Smith (1973). These authors have suggested that detection of rectangular bars, beyond the region of initial threshold decline, is mediated by edge detection.

Main experiment: Threshold as a function of the width of truncated sine-wave gratings

In the main experiment, test stimuli were truncated 3.0 c/deg sine-wave gratings, symmetrically positioned with respect to the fixation point (cosine phase) (see Fig. 1). They ranged in width from 2.3' to 4.6°. The 2.3' stimulus, representing only about 12% of a cycle, was indistinguishable from a narrow luminance bar, while the 4.6° stimulus contained nearly 14 cycles. Since the full display subtended 5°, there were always margins consisting of the uniform field. Test stimuli were superimposed on 3.0 c/deg pedestal gratings, maintained at threshold contrast, which acted to facilitate detection of the test stimuli. They were present in both intervals of forced choice trials, so that they could not cue a correct response.

Contrast thresholds were measured in two stages. In the first, (●) symbols in Fig. 4, threshold estimates were obtained for 11 test widths ranging from 2.3' to 40' for the two emmetropic subjects, AA and JK, in each of 4 separate sessions. The resulting 8 estimates at each width, composed of 440 forced-choice trials, were averaged (see Experimental procedure). In the second stage, (×) symbols in Fig. 4, threshold estimates were obtained for 15 test widths ranging from 7' to 4.6° for the same two subjects, in each of 3 separate sessions. The resulting 6 estimates were averaged. The overlap values in the two sets of measurements (7', 14', 21' and 40') were used to combine the data into a single function.

The results are displayed in Fig. 4. The solid curve through the data is the fit of a model incorporating a receptive field shape and the effects of probability summation over space. From 2.3' to 40' the curve is rather jagged, presumably reflecting characteristics of both the summative process and the test stimuli. For instance, the flat portion near 10' is undoubtedly due to the relatively small contribution to the integrated stimulus flux for width increments near 10'. 10' represents the width of the test stimulus at which the addition of dark flanks on either side of the central light half-cycle begins (see Fig. 1). Since a width

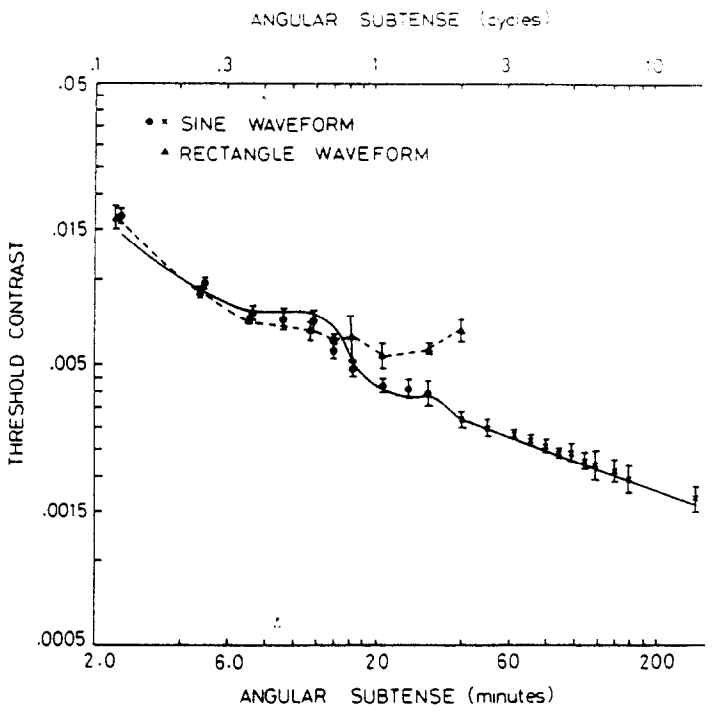

Fig. 4. Threshold as a function of test stimulus width. Filled circles and crosses represent threshold contrasts for truncated 3.0 c/deg sine-wave gratings (cosine phase) of the indicated width. (●) are the geometric means of 8 threshold estimates (4 each from 2 subjects), and (×) are the geometric means of 6 threshold estimates (3 each from 2 subjects). Each estimate was computed from a block of 55 forced-choice trials. The error bars represent ±1 S.E. The solid curve through (●) and (×) symbols is the fit of the model based on probability summation in space across receptive fields. The best fitting straight line through the (×) symbols (least-squares criterion) has slope −0.35 ± 0.01. The triangles represent analogous data for rectangle waveforms and are each based on 4 threshold estimates. 2 from each subject. Data are for subjects JK and AA.

increment in the cosine function at 10′ is near a zero-crossing, its stimulus effect will be small. Glezer and Kostelyanets (1975) observed similar "flat" portions for the detection of truncated square-wave gratings, but attributed them to the underlying receptive field process. From 40′ to 4.6° the threshold data in log–log coordinates lie along a best fitting straight line of slope −0.35 with standard error 0.01 (formula for standard error of slope given by Mansfield, 1973).

In Fig. 5 the sine-wave grating data of Fig. 4 are replotted (●) as a function of the number of cycles in the test stimulus. Also shown are data from four other studies (Estevez and Cavonius, 1976; Hoekstra *et al.*, 1974; Savoy and McCann, 1975; J. G. Robson, as reported by Mostafavi and Sakrison, 1976), scaled vertically to have equal ordinate values at 2.0 cycles. Table 1 summarizes the conditions under which the data were collected. Data were chosen for comparison which most nearly matched the conditions of the present study. There is a lack of convergence of the results. For Savoy and McCann (1975), an increase in the number of cycles in the horizontal direction was accompanied by a corresponding elongation of the patterns in the vertical direction. Assuming probability summation over space, a steeper threshold decline would be expected under their conditions. Estevez and Cavonius have argued that the more precipitous decline in threshold observed by Hoekstra *et al.* (1974) and Savoy and McCann (1975) may be due to artifacts introduced by their surround conditions. In support of this suggestion, data of Estevez and Cavonius, Robson, and those of the present study, in which surround conditions were identical, bear the greatest similarity. The three studies found a slow, regular decline in threshold as a function of the number of cycles. The data points from Robson and from the present study lie very close together, but those of Estevez and Cavonius exhibit a somewhat shallower decline. An explanation for this difference is not apparent.

Space domain properties of the 3.0 c/deg channel

The truncated sine-wave data of Fig. 4 will be used to obtain the receptive field shape of the detectors comprising the 3.0 c/deg channel, and to characterize the means by which their responses are combined as probability summation in space. Probability summation is the increasing probability with increasing number of stimulated receptive fields that a signal will be detected, given the variability of receptive field response.

Assume that properly oriented, symmetrical receptive fields are continuously distributed in position along the horizontal. (That there must be a finite sampling density will not affect the derivation, since the sampling density is sufficiently large to be indis-

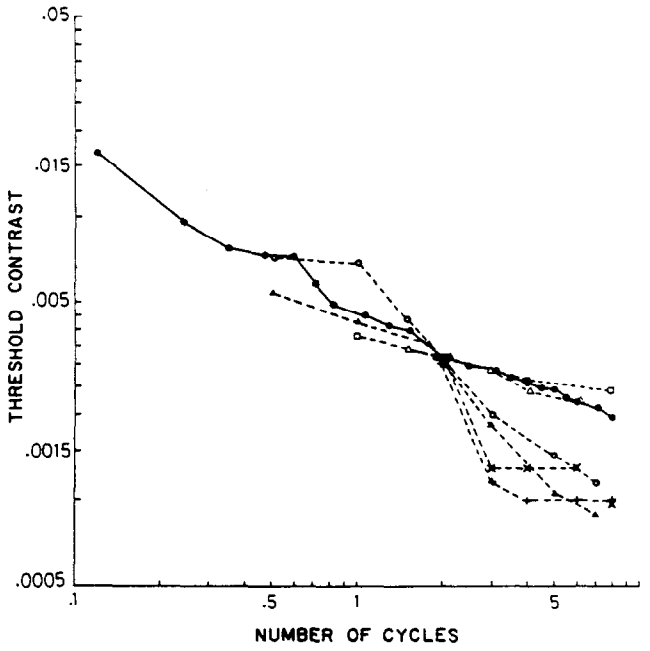

Fig. 5. Comparison of several studies. The sine-wave threshold data of Fig. 4 are replotted (filled circles) as a function of the number of cycles of the test stimulus. Also shown are comparable data from four other studies: (+, ×), Hoekstra *et al.* (1974); (▲, ○), Savoy and McCann (1975); (□) Estevez and Cavonius (1976); (△) Robson, as reported by Mostafavi and Sakrison (1976). See Table 1.

tinguishable from a continuum to psychophysical measurement.) Evidence for the linearity of spatial summation dictates that the response R of a receptive field at position x to a stimulus waveform L of contrast C and width w, be given by the value of the convolution:

$$R(x, w) = \int_{-x}^{x} CL(y, w)S(x - y)\,dy \qquad (1)$$

where $S(y)$ is the receptive field sensitivity function to be determined. The truncated sine-wave stimulus of width w may be expressed:

$$L(y, w) = \begin{bmatrix} \cos 2\pi f y, & |y| \leqslant w/2 \\ 0, & |y| > w/2 \end{bmatrix}$$

where f is the frequency of the stimulus. Let the probability that a response R of a detector exceeds a criterion threshold level be given by the "probability-of-seeing" function:

$$f(R) = 1 - \exp(-\alpha|R|^{\beta}) \qquad (2)$$

where α is a scale factor, and β characterizes the steepness of the probability-of-seeing function (Green and Luce, 1975). This expression has been chosen because it is computationally convenient and because it fits empirical probability-of-seeing functions. If the signal is detected whenever a response exceeds the criterion level, and if the false positive rate is assumed to be negligible, threshold contrast C_t as a function of stimulus width is given by (see Appendix):

$$C_t(w) \propto \left(\int_{-x}^{x} \left| \left[\int_{-x}^{x} L(y, w)S(x - y)dy \right] \right|^{\beta} dx \right)^{-1/\beta} \qquad (3)$$

In Eqn 3, the threshold function $C_t(w)$ is proportional to a double integration. The integral in square brackets is the convolution which describes the linear spatial summation within a receptive field. The outer integral, taken over all spatial positions x, describes the effects of probability summation, and is characterized by the parameter β.

Quick (1974), and Graham and Rogowitz (1976) have pointed out that the form of the probability summation here discussed is mathematically equivalent to assuming nonlinear transformation of the linear outputs, followed by spatial integration. Mostafavi and Sakrison (1976) have adopted this interpretation in modelling the angular and radial bandwidths of a spatial frequency channel.

Probability summation. For truncated sine-wave luminance profiles whose width w increases in half-cycle steps, (×) symbols in Fig. 4, Eqn 3 requires that $C_t(w)$ vs w in log–log coordinates will be asymptotically straight with slope $-1/\beta$. The (×) symbols in Fig. 4 do lie along a straight line having slope -0.35. Hence, if the model is correct, the parameter β of the probability-of-seeing function should have the value $\beta = 1/0.35 = 2.87$. Using a two-alternative forced-choice procedure, Foley and Legge (unpublished data) have measured probability-of-seeing functions for gratings of 3 spatial frequencies. In all cases, the steepness parameter β is close to 3. Furthermore, since the shape of probability-of-seeing functions for contrast detection are independent of duration (Nachmias, 1967), as well as many other stimulus variables (Blackwell, 1963), it is predicted that probability summation in time should also be characterized by an asymptotic threshold curve of slope—$1/\beta$. This turns out to be the case. For stimulus durations beyond

Table 1. Stimulus conditions for the measurements displayed in Fig. 5

Symbol	Source	Mean luminance (cd/m^2)	Spatial frequency (c/deg)	Stimulus duration (msec)	Procedure	Surround conditions
+	Hoekstra *et al.* (1974); Fig. 1, Subject 1	2.0	2.0	continuous	method of adjustment	dark surround
×	Hoekstra *et al.* (1974); Fig. 1, Subject 2	2.0	2.0	continuous	method of adjustment	dark surround
▲	Savoy and McCann (1975); Fig. 4(I), one subject	9.3	*	continuous	method of adjustment	9.3 cd/m^2 homogeneous, but with narrow, visible borders
○	Savoy and McCann (1975); Fig. 4(II), same subject	9.3	*	continuous	method of adjustment	dark surround
□	Estevez and Cavonius (1976); Fig. 2, two subjects	7.0	several	continuous	method of limits	homogeneous, 7.0 cd/m^2
●	Legge (present study); two subjects	4.6	3.0	250	forced choice	homogeneous, 4.6 cd/m^2
△	Robson, see Mostafavi and Sakrison (1976); Fig. 6	500	1.2†	100	yes–no staircase	homogeneous, 500 cd/m^2

* The spatial frequency varied with the number of cycles.
† Threshold curves at several other spatial frequencies had very similar shapes.

111 msec, contrast threshold as a function of duration for 3.0 c/deg sine-wave gratings is best fit by a straight line in log–log coordinates with slope −0.34 (Legge, 1978). The convergence of results from the measurements of probability-of-seeing functions, threshold as a function of stimulus width, and threshold as a function of stimulus duration, suggests that probability summation is the means by which information is combined across time and space in the detection of 3.0 c/deg gratings.

King-Smith and Kulikowski (1975) have argued similarly that the detection of a rectangle-wave grating consisting of fine lines with 15′ spacings, can be accounted for by the activation of a set of line detecting mechanisms, together with probability summation across space.

Hilz and Cavonius (1974), and Robson (1975) have shown that contrast sensitivity at all spatial frequencies decreases with increasing retinal eccentricity. According to Robson, as reported by Mostafavi and Sakrison (1976), the decline in sensitivity at the spatial frequencies tested is governed by the function

$$\exp(-n/26.06).$$

n is the test patch's distance from the point of fixation, measured in the number of cycles of the test frequency. In the present study, test stimuli never extended beyond 7 cycles from the point of fixation, a distance at which the attenuation factor is 0.76. Most of the stimuli did not extend beyond 2 cycles, a distance at which the attenuation factor is only 0.93. These effects are small compared with the observed decrease in threshold, and would oppose the effects of probability summation. Accordingly, it is concluded that effects of retinal inhomogeneity do not affect the probabilistic interpretation of the asymptotic threshold decline in Fig. 4.

Receptive field sensitivity function. With a value of β in hand, Eqn 3 may, in principle, be solved for the receptive field sensitivity function $S(y)$, since the other functions are known. However, an analytical solution could not be found, so an approximate solution was obtained (see Appendix). The effects of probability summation (outer integral in Eqn 3), were approximated by the multiplication of the inner integral by the function $w^{1/\beta}$. The receptive field sensitivity was then related to the change in threshold per increment of stimulus width, and is thus related to the derivative of the threshold curve. The method is similar to one used by Kincaid *et al.* (1960).

One side of the resulting symmetrical receptive field sensitivity function is plotted in Fig. 6. The points were derived by numerical differentiation and a smooth curve drawn through them. The receptive field possesses an excitatory center, inhibitory flanks, and weak, peripheral, excitatory zones.

The validity of the approximation used in obtaining the receptive field function in Fig. 6 was checked. The function was used in Eqn 3 to generate a threshold curve. This is the solid curve through the data in Fig. 4. The fit is good. Hence, the complicated threshold curve of Fig. 4 may be accounted for by the two processes of (i) spatial summation within the receptive field of Fig. 6, and (ii) probability summation in space across receptive fields, characterized by the parameter β with value near 3.

An alternative interpretation for the data of Fig. 4 exists. It attributes the entire threshold decline to a very broad receptive field with many excitatory and inhibitory lobes, but with no probability summation. This interpretation is deemed unlikely, however, in view of the aforementioned convergent evidence for probability summation over space, and the implausibility that the visual system suppresses the advantages in detection accruing from probability summation.

Also drawn in Fig. 6 are sensitivity functions due to King-Smith and Kulikowski (1975) (dotted curve), and Blakemore and Campbell (1969) (dashed curve). The sensitivity curve of King-Smith and Kulikowski (1975) is the Fourier transform of the grating sensitivity of a fine line detector, with effects of probability summation removed. In terms of the analysis of the present paper, it is the receptive field structure of the most sensitive spatial frequency channel. Blakemore and Campbell (1969) have shown that tuning curves obtained from spatial frequency adaptation may be represented by scaled versions of the function $(e^{-f^2} - e^{-4f^2})^2$. After right–left inversion of this func-

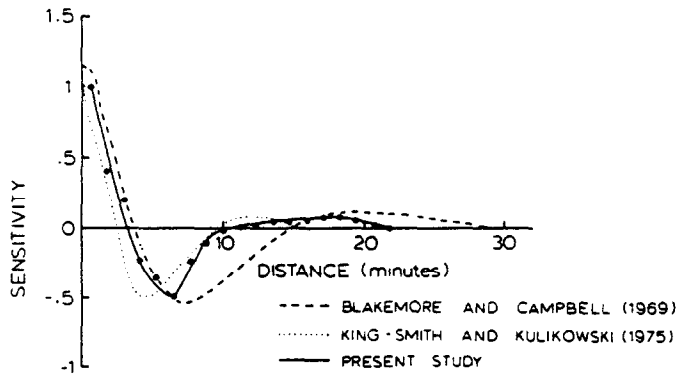

Fig. 6. Receptive field sensitivity functions. The solid curve is one side of the symmetrical receptive field sensitivity function which was derived from the data of Fig. 4 using the methods described in the Appendix. Values represented by filled circles were computed numerically. Dashed curve: sensitivity function derived from the spatial frequency adaptation tuning functions of Blakemore and Campbell (1969) by Stromeyer and Klein (1974). Dotted curve: Sensitivity profile derived by King-Smith and Kulikowski (1975) from the grating sensitivity of fine line detectors.

tion and Fourier transformation (Stromeyer and Klein, 1974), the spatial sensitivity of the adapted channel is obtained. Such a function is plotted as the dashed curve in Fig. 6. (Computations were by Stromeyer and Klein, 1974). There is considerable similarity between the three curves. All three curves show peripheral, excitatory zones. The King-Smith and Kulikowski curve is narrower than the others, but this may be a result of their use of fine lines in the derivation of the sensitivity profile.

Acknowledgements—I wish to thank Dr R. J. W. Mansfield, Professor David M. Green, and Dr C. F. Stromeyer III for their very helpful comments, suggestions, and criticisms. I also wish to thank Amy Aldrich, Janice Kilpatrick and Wendy Willson Legge. I am grateful to Scott Bradner, who designed and constructed the circuitry necessary to produce the displays. I thank the National Research Council of Canada for a postgraduate scholarship, and the Medical Research Council of Canada for a postdoctoral fellowship. The work was supported in part by NSF Research Grant BNS75-08437 to Dr Mansfield. The study reported here formed part of a doctoral dissertation submitted to Harvard University. The paper was completed at The Physiological Laboratory, University of Cambridge, Cambridge, England.

REFERENCES

Bagrash F. M. (1973) Size-selective adaptation: psychophysical evidence for size tuning and effects of stimulus contour and adapting flux. *Vision Res.* **13**, 575–598.

Blackwell H. R. (1963) Neural theories of simple visual discrimination. *J. opt. Soc. Am.* **53**, 129–160.

Blakemore C. and Campbell F. W. (1969) On the existence of neurones in the human visual system selectively sensitive to the orientation and size of retinal images. *J. Physiol., Lond.* **203**, 237–260.

Campbell F. W. and Green D. G. (1965) Optical and retinal factors affecting visual resolution. *J. Physiol., Lond.* **181**, 576–593.

Campbell F. W. and Gubisch R. W. (1966) Optical quality of the human eye. *J. Physiol., Lond.* **186**, 558–578.

Campbell F. W. and Robson J. G. (1968) Application of Fourier analysis to the visibility of gratings. *J. Physiol., Lond.* **197**, 551–566.

Campbell F. W., Carpenter R. H. S. and Levinson J. Z. (1969) Visibility of aperiodic patterns compared with that of sinusoidal gratings. *J. Physiol., Lond.* **204**, 283–298.

Cohn T. W., Thibos L. N. and Kleinstein R. N. (1974) Detectability of a luminous increment. *J. opt. Soc. Am.* **64**, 1321–1327.

Estevez O. and Cavonius C. R. (1976) Low-frequency attenuation in the detection of gratings: sorting out the artifacts. *Vision Res.* **16**, 497–500.

Fiorentini A. (1971) Excitatory and inhibitory interactions in the human eye. In *Visual Sciences: Proceedings of the 1968 International Symposium* (edited by Pierce J. R. and Levine J. R.), pp. 269–283. Indiana University Press, Bloomington, Indiana.

Glezer V. D. and Kostelyanets N. B. (1975) The dependence of threshold for perception of rectangular gratings upon stimulus size. *Vision Res.* **15**, 753–756.

Graham N. and Nachmias J. (1971) Detection of grating patterns containing two spatial frequencies: a comparison of single-channel and multiple-channel models. *Vision Res.* **11**, 251–259.

Graham N. and Rogowitz B. E. (1976) Spatial pooling properties deduced from the detectability of FM and quasi-AM gratings: a reanalysis. *Vision Res.* **16**, 1021–1026.

Graham C. H., Brown R. H. and Mote F. A. (1939) Relation of size of stimulus and intensity in the human eye. I: intensity thresholds for white light. *J. exp. Psychol.* **24**, 555–573.

Green D. M. and Luce R. D. (1975) Parallel psychometric functions from a set of independent detectors. *Psychol. Rev.* **82**, 483–486.

Hilz R. and Cavonius C. R. (1974) Functional organization of the peripheral retina: sensitivity to periodic stimuli. *Vision Res.* **14**, 1333–1337.

Hines M. (1976) Line spread function variation near the fovea. *Vision Res.* **16**, 567–572.

Hoekstra J., van der Goot D. P. J., van den Brink G. and Bilsen F. A. (1974) The influence of the number of cycles upon the visual contrast threshold for spatial sine-wave patterns. *Vision Res.* **14**, 365–368.

Kincaid W. M., Blackwell H. R. and Kristofferson A. H. (1960) Neural formulation of the effect of target size and shape upon visual detection. *J. opt. Soc. Am.* **50**, 143–148.

King-Smith P. E. and Kulikowski J. J. (1975) The detection of gratings by independent activation of line detectors. *J. Physiol., Lond.* **247**, 237–271.

Krauskopf J. (1962) Light distribution in human retinal images. *J. opt. Soc. Am.* **52**, 1046–1050.

Kulikowski J. J. and King-Smith P. E. (1973) Spatial arrangement of line, edge and grating detectors revealed by subthreshold summation. *Vision Res.* **13**, 1455–1478.

Legge G. E. (1976a) Adaptation to a spatial impulse: implications for Fourier transform models of visual processing. *Vision Res.* **16**, 1407–1418.

Legge G. E. (1976b) *Contrast Detection in Human Vision: Spatial and Temporal Properties*. Ph.D. thesis, Harvard University.

Legge G. E. (1978) Sustained and transient mechanisms in human vision: temporal and spatial properties. *Vision Res.* **18**, 69–81.

Macleod I. D. G. and Rosenfeld A. (1974) The visibility of gratings: spatial frequency channels or bar detecting units? *Vision Res.* **14**, 909–915.

Mansfield R. J. W. (1973) Brightness function: effect of area and duration. *J. opt. Soc. Am.* **63**, 913–920.

Matin L. (1975) Ricco's Law: the response as a power function of stimulus luminance and distance from target center. *Vision Res.* **15**, 1381–1384.

Mostafavi H. and Sakrison D. J. (1976) Structure and properties of a single channel in the human visual system. *Vision Res.* **16**, 957–968.

Nachmias J. (1967) The effect of exposure duration on visual contrast sensitivity with square-wave gratings. *J. opt. Soc. Am.* **57**, 421–427.

Nachmias J. and Kocher E. C. (1970) Visual detection and discrimination of luminance increments. *J. opt. Soc. Am.* **60**, 382–389.

Nachmias J. and Sansbury R. V. (1974) Grating contrast: discrimination may be better than detection. *Vision Res.* **14**, 1039–1042.

Pantle A. and Sekuler R. (1968) Size detecting mechanisms in human vision. *Science, N.Y.* **162**, 1146–1148.

Quick R. F. (1974) A vector-magnitude model of contrast detection. *Kybernetik* **16**, 65–67.

Riggs L. A., Armington J. C. and Ratliff F. (1954) Motions of the retinal image during fixation. *J. opt. Soc. Am.* **44**, 315–321.

Robson J. G. (1975) Regional variation of contrast sensitivity in the visual field. ARVO spring meeting, Sarasota, Florida.

Savoy R. L. and McCann J. J. (1975) Visibility of low-spatial-frequency sine-wave targets: dependence on number of cycles. *J. opt. Soc. Am.* **65**, 343–350.

Schade O. H. Sr (1956) Optical photoelectric analog of the eye. *J. opt. Soc. Am.* **46**, 721–739.

Shapley R. (1974) Gaussian bars and rectangular bars: the

influence of width and gradient on visibility. *Vision Res.* **14**, 1457–1461.
Stromeyer C. F. III and Julesz B. (1972) Spatial frequency masking in vision: critical bands and spread of masking. *J. opt. Soc. Am.* **62**, 1221–1232.
Stromeyer C. F. III and Klein S. (1974) Spatial frequency channels in human vision as asymmetric (edge) mechanisms. *Vision Res.* **14**, 1409–1420.
Thomas J. P. (1968) Linearity of spatial integration involving inhibitory interactions. *Vision Res.* **8**, 49–60.
Thomas J. P. (1970) Model for function of receptive fields in human vision. *Psychol. Rev.* **77**, 121–134.
Westheimer G. (1965) Spatial interaction in the human retina during scotopic vision. *J. Physiol., Lond.* **181**, 881–894.
Westheimer G. (1967) Spatial interaction in human cone vision. *J. Physiol., Lond.* **190**, 139–154.
Westheimer G. and Campbell F. W. (1962) Light distribution in the image formed by the living human eye. *J. opt. Soc. Am.* **52**, 1040–1045.
Westheimer G. and Wiley W. R. (1970) Distance effects in human scotopic retinal interaction. *J. Physiol., Lond.* **206**, 129–143.
Wetherill G. B. and Levitt H. (1964) Sequential estimation of points on a psychometric function. *Br. J. Math. Stat. Psych.* **18**, 1–10.

APPENDIX: DERIVING AND SOLVING EQUATION 3

Deriving Eqn 3

Legge (1978) has shown that, if the probability-of-seeing function has the form given in Eqn 2, and if a probability summation model is assumed, the following equation holds for the probability of detection of a stimulus pattern:

$$P_{\text{detect}} = 1 - \exp\left[\int_{-x}^{x}\left|\int_{-x}^{x} CL(y, w)S(x-y)\,dy\right|^{\beta} dx\right]$$

An experimental procedure was used which estimated contrasts for a fixed probability of detection as a function of stimulus width w. Such a fixed probability holds when the argument of the exponential remains constant. Hence, the condition for threshold contrast C_t is:

$$\int_{-x}^{x}\left|\int_{-x}^{x} C_t L(y, w)S(x-y)\,dy\right|^{\beta} dx = \text{const.}$$

Or:

$$C_t(w) \propto \left[\int_{-x'}^{x'}\left|\int_{-x'}^{x'} L(y, w)S(x-y)\,dy\right|^{\beta} dx\right]^{-1/\beta}$$

This is Eqn 3.

Solving Eqn 3

As discussed in the text, the asymptotically straight portion of $C_t(w)$ has slope $-1/\beta$. The measured slope was -0.35 and therefore $\beta = 2.87$. With β known, Eqn 3 can be solved for the sensitivity function $S(y)$, because the functions $C_t(w)$ and $L(y, w)$ are known. However, an analytical solution could not be found. Accordingly, the following approximation was used. The effects of probability summation—namely, raising the convolution integral to the power β and integrating over space—were approximated by multiplying the convolution integral by the function $w^{1/\beta}$:

$$C_t(w)\left[\int_{-x'}^{x'} L(y, w)S(y)\,dy\right]w^{1/\beta} \approx \text{const.}$$

[Under some conditions (Legge, 1978), this approximation is exact. In general, the approximation can be justified only by the goodness of fit provided by the approximate solution to the data.]
and:

$$[C_t(w)\,w^{1/\beta}]^{-1} \propto \int_{-x}^{x} L(y, w)S(y)\,dy.$$

Calling the integral on the right $I(w)$ and inserting the truncated sinewave stimulus:

$$I(w) = \int_{-w/2}^{w/2} \cos 2\pi f y S(y)\,dy.$$

By differentiating $I(w)$, the sensitivity S can be found.

$$dI(w)/dw = \frac{d}{dw}\left(\int_{-w/2}^{w/2} \cos 2\pi f y S(y)\,dy\right)$$

$$= \cos \pi f w S(w/2)$$

$$S(w/2) = \frac{1}{\cos \pi f w}\frac{dI(w)}{dw}$$

$$= \frac{1}{\cos \pi f w}\frac{d}{dw}[C_t(w)w^{1/\beta}]^{-1}.$$

Hence, the weighting function S is given as the derivative of a known function. Numerical derivatives were taken to obtain S, and the points are plotted in Fig. 6. The approximation was checked by using S to compute the threshold curve from Eqn 3. The solid curve through the data in Fig. 4 is the result. The fit is good.